Supplement of Atmos. Chem. Phys., 20, 11527–11550, 2020
https://doi.org/10.5194/acp-20-11527-2020-supplement

Atmospheric Chemistry and Physics
Open Access
EGU

Supplement of

Measurement report: Characterization of severe spring haze episodes and influences of long-range transport in the Seoul metropolitan area in March 2019

Hwajin Kim et al.

Correspondence to: Hwajin Kim (hjkim@kist.re.kr)

Table S1. Average (± 1 standard deviation), minimum and maximum concentrations of the particulate matter (PM_1) species and the total PM_1 mass over the whole campaign, and the average contribution of each of the PM_1 species to the total PM_1 mass.

	Average conc. ± one standard deviation (μg m^{-3})	Minimum conc. (μg m^{-3})	Maximum conc. (μg m^{-3})	Fraction of total PM_1 (%)	Detection limit (3min/ 6min) (μg m^{-3})
Organics	13.3 ± 7.51	1.29	45.0	38	0.03/0.02
Nitrate	10.6 ± 9.68	0.21	52.0	30	0.01/0.01
Sulfate	4.20 ± 3.49	0.60	20.0	12	0.01/0.01
Ammonium	4.70 ± 3.99	0.28	21.2	13	0.02/0.01
Chloride	0.60 ± 0.54	0	4.03	2	0.00/0.00
Black carbon	1.60 ± 0.93	0.05	5.55	5	0.1/0.05
Total PM_1	35.1 ± 23.8	3.85	129	-	0.05/0.03

Table S2. Comparison of the average O/C, H/C, and OM/OC ratios of total OA and the four OA factors identified from PMF analysis calculated using the Aiken-Ambient method (Aiken et al., 2008) and the improved Canagaratna-Ambient method (Canagaratna et al.,2015) .

Species	Ratio	Aiken-Ambient	Canagaratna-Ambient
OA	O/C	0.41	0.52
	H/C	1.45	1.61
	OM/OC	1.70	1.86
HOA	O/C	0.08	0.10
	H/C	1.97	1.88
	OM/OC	1.29	1.33
COA	O/C	0.10	0.12
	H/C	1.74	1.88
	OM/OC	1.29	1.33
SFOA	O/C	0.41	0.53
	H/C	1.41	1.55
	OM/OC	1.71	1.87
LO-OOA1	O/C	0.47	0.59
	H/C	1.45	1.61
	OM/OC	1.76	1.93
LO-OOA2	O/C	0.50	0.65
	H/C	1.45	1.62
	OM/OC	1.81	2.02
MO-OOA1	O/C	0.99	0.99
	H/C	1.56	1.56
	OM/OC	2.46	2.46
MO-OOA2	O/C	0.93	1.11
	H/C	1.20	1.32
	OM/OC	2.44	2.69

Table S3. Expected (deLaeter et al., 2003) and calculated lead isotopic ratios (m) and Pearsons R.

		Open signal				Closed signal			
		V-mode		W-mode		V-mode		W-mode	
	Natural Isotope Ratio	m	R	m	R	m	R	m	R
$^{206}Pb^{+}/^{208}Pb^{+}$	0.46	0.48	0.92	0.41	0.63	0.44	0.84	0.32	0.36
$^{207}Pb^{+}/^{208}Pb^{+}$	0.422	0.45	0.77	0.37	0.5	0.36	0.42	0.22	0.18
$^{206}Pb^{++}/^{208}Pb^{++}$	0.46	0.29	0.06	0.35	0.08	.	.	0.04	0
$^{207}Pb^{++}/^{208}Pb^{++}$	0.422	0.4	0.33	0.01	0.03	0.05	0.39	0.01	0.02

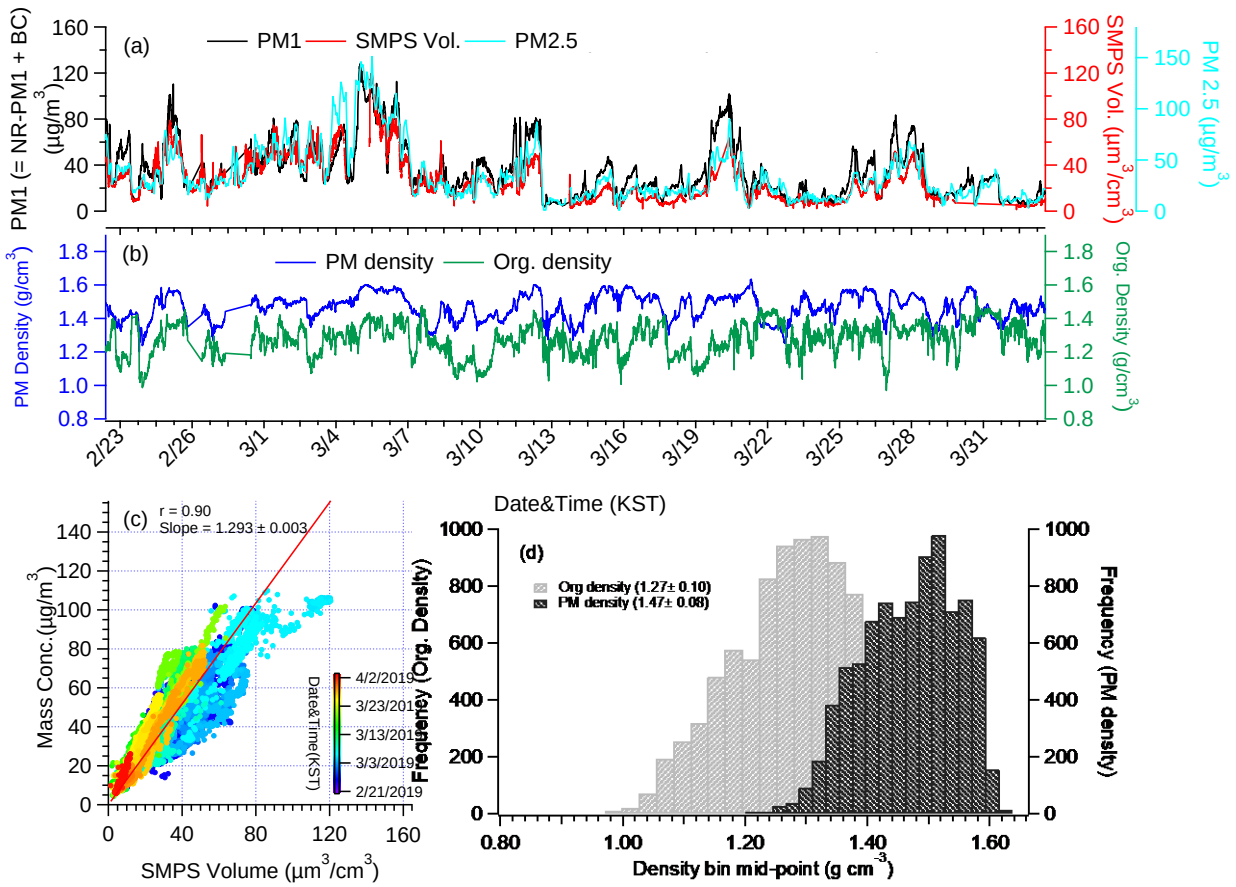

Figure S1. (a) Time series of total particulate matter (PM_1), scanning mobility particle sizer (SMPS) volume concentrations and PM2.5 mass concentration measured at Gireum site ; **(b)** Time series of the organic aerosol density estimated using the method reported in Kuwata et al. (2012)

$$\rho_{org} = [12 + 1\bullet(H/C) + 16\bullet(O/C)]/ [7 + 5\bullet(H/C) + 4.15\bullet(O/C)]$$

and bulk aerosol density estimated from the measured chemical composition, known inorganic species density and the organic density estimated above (Zhang et al., 2015) . **(c)** Scatter plot of the total PM_1 mass (NR-PM_1 plus BC) versus SMPS volume, where the NR-PM_1 mass concentrations have been determined using the composition-dependent collection efficiencies; **(d)** histogram of organic aerosol density (average = 1.27 g cm^{-3}) and bulk aerosol density (average = 1.47 g cm^{-3}).

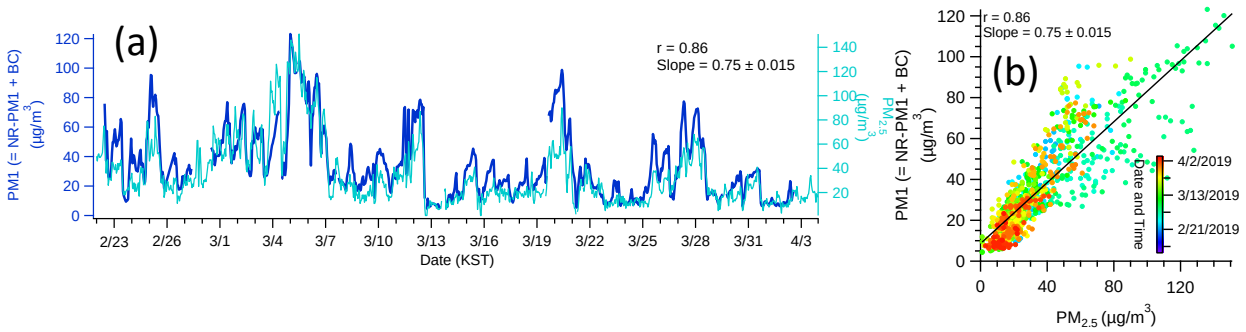

Figure S2. (a) Time series of total particulate matter (PM1) concentration and $PM_{2.5}$ mass concentration measured at Gireum site (b) Scatter plot of total PM1 mass (NR-PM_1 plus BC) versus $PM_{2.5}$ mass.

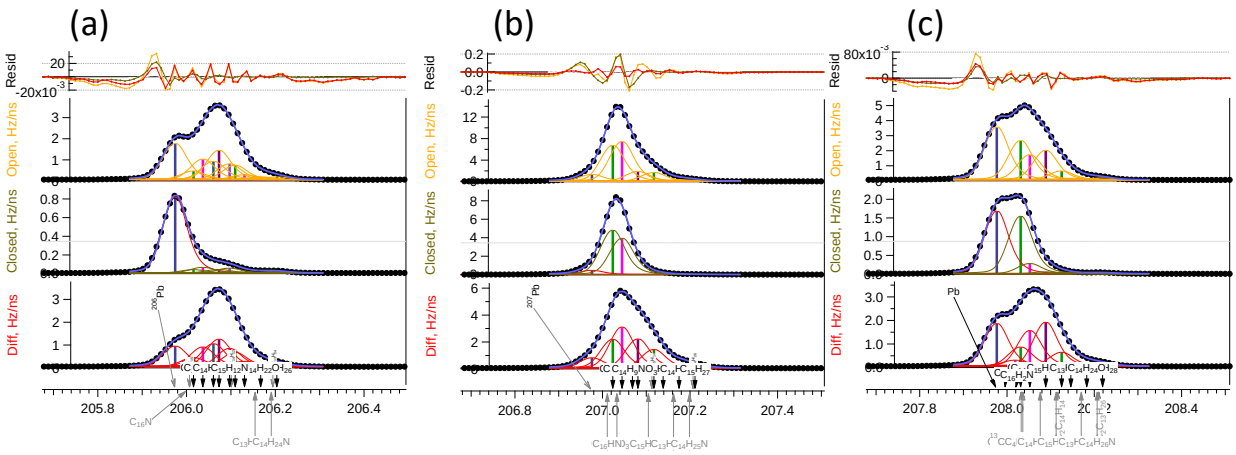

Figure S3. 2.5 minute averaged open V mode mass spectra at (a) m/z 206, (b) m/z 207 and (c) m/z 208 for $^{206}Pb^{+}$,$^{207}Pb^{+}$ and $^{208}Pb^{+}$. during Haze period at KIST site. Black lines (behind of the purple line) and circles correspond to the HR-AMS raw signal. Yellow (open), dark green(closed) and red(diff) are modified Gaussian functions that represent the signal of individuals ions whose exact mass is indicated by the vertical lines. The height of the vertical lines corresponds to the peak height of the modified Gaussian functions. Purple lines are the sum of the individual ion peaks and represent the fitted total signal at the given nominal m/z.

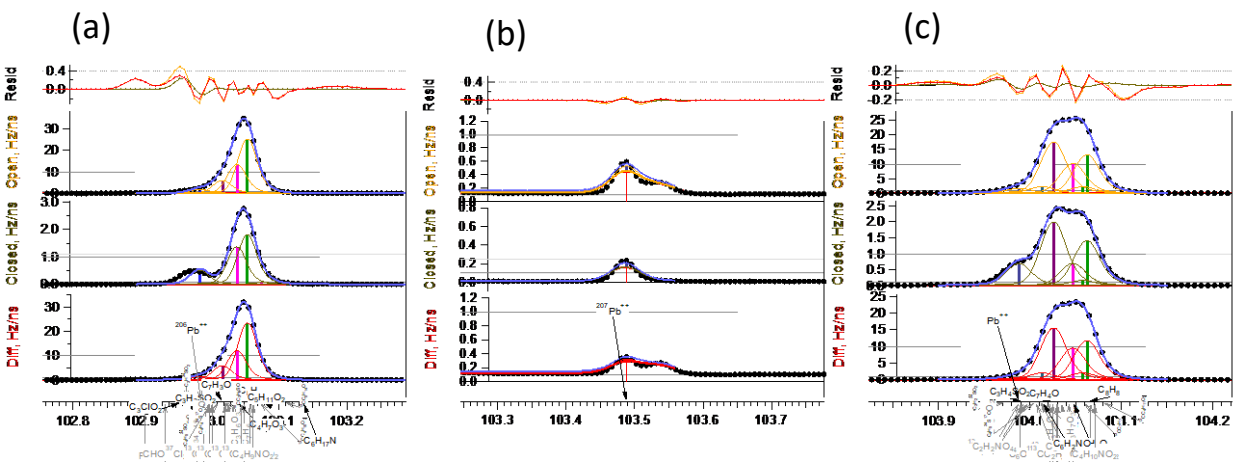

Figure S4. 2.5 minute averaged open V mode mass spectra at (a) m/z 103, (b) m/z 103.5 and (c) m/z 104 for $^{208}Pb^{++}$, $^{207}Pb^{++}$ and $^{206}Pb^{++}$, during Haze period at KIST site. Black lines (behind of the purple line) and circles correspond to the HR-AMS raw signal. Yellow (open), dark green(closed) and red(diff) are modified Gaussian functions that represent the signal of individuals ions whose exact mass is indicated by the vertical lines. The height of the vertical lines corresponds to the peak height of the modified Gaussian functions. Purple lines are the sum of the individual ion peaks and represent the fitted total signal at the given nominal m/z.

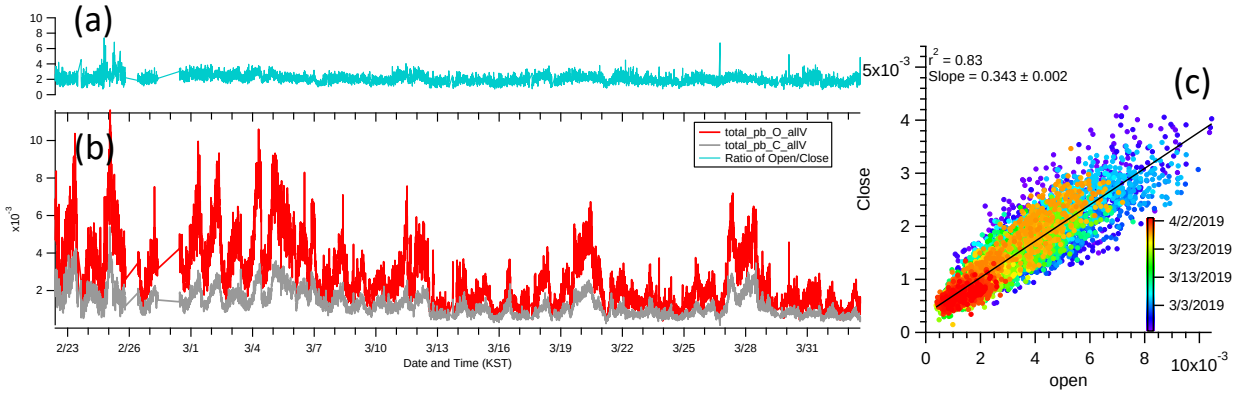

Figure S5. (a,b) Time series of total open (red) and closed (black) signal of lead from Vmode and the ratio between open and close (turquoise) total signal of lead from V mode; and **(c)** Scatter plot of total open and close signal of lead from Vmode data. Note that total open and close signals were calculated as the sum of the $^{208}Pb^{+}$, $^{207}Pb^{+}$, $^{206}Pb^{+}$, $^{208}Pb^{++}$, $^{207}Pb^{++}$ and $^{206}Pb^{++}$.

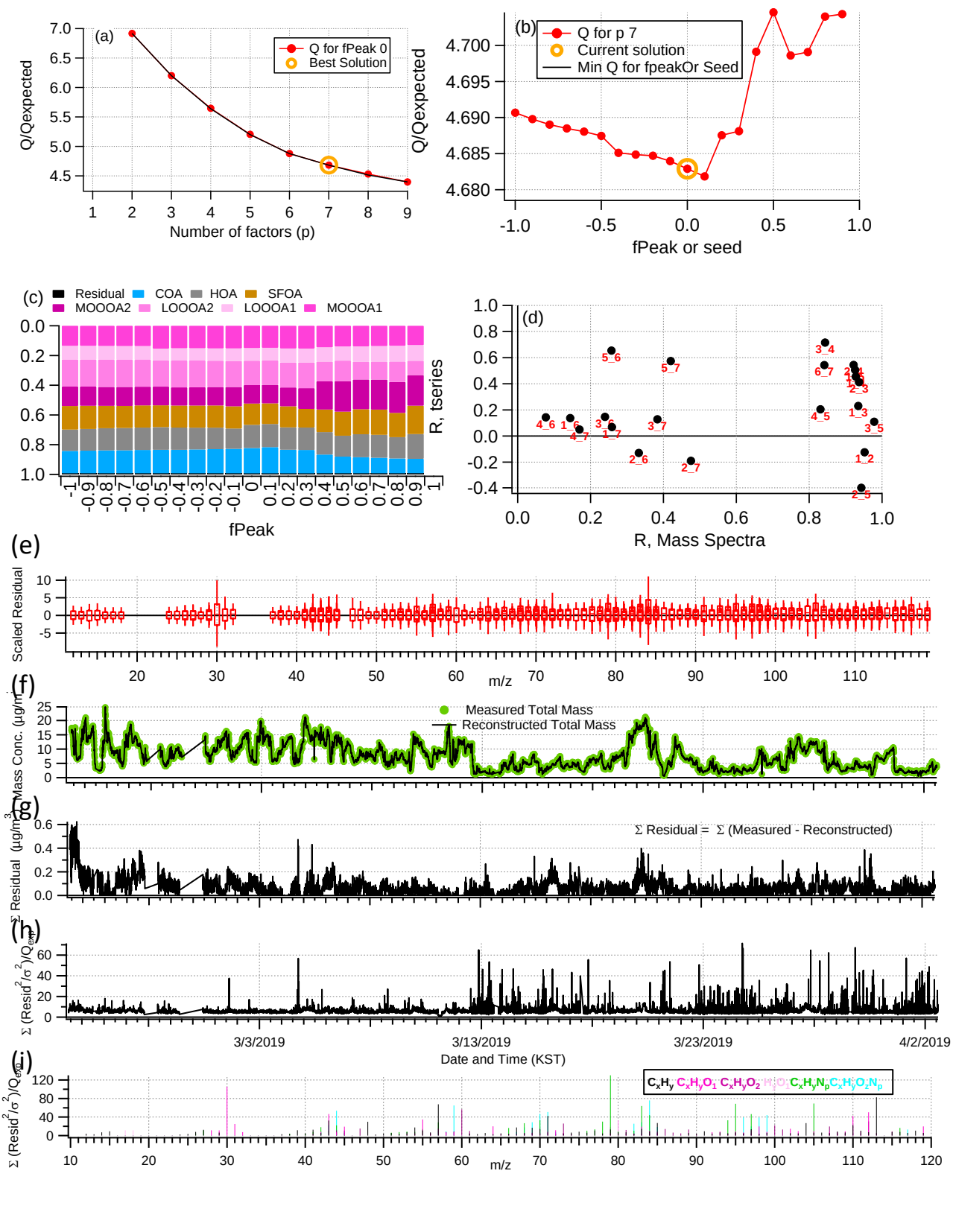
(a)
Q for fPeak 0
Best Solution
Q/Qexpected
Number of factors (p)
(b)
Q for p 7
Current solution
Min Q for fpeakOr Seed
Q/Qexpected
fPeak or seed
(c)
Residual
COA
HOA
SFOA
MOOOA2
LOOOA2
LOOOA1
MOOOA1
Mass fraction
fPeak
R, tseries
(d)
R, Mass Spectra
(e)
Scaled Residual
m/z
(f)
Measured Total Mass
Reconstructed Total Mass
Mass Conc. (µg/m3)
(g)
Σ Residual = Σ (Measured - Reconstructed)
Σ Residual (µg/m3)
(h)
Σ (Resid2/σ2)/Qexp
3/3/2019
3/13/2019
3/23/2019
4/2/2019
Date and Time (KST)
(i)
Σ (Resid2/σ2)/Qexp
m/z

Figure S6. Summary of the key diagnostic plots of the chosen 7-factor from PMF analysis of the organic aerosol fraction: **(a)** Q/Q_{exp} as a function of the number of factors (p) explored in PMF analysis, with the best solution denoted by the open orange circle. Plots **b-i** are for the chosen solution set, containing 7 factors: **(b)** Q/Q_{exp} as a function of fPeak; **(c)** mass fractional contribution to the total mass of each of the PMF factors, including the residual (in purple), as a function of fPeak; **(d)** Pearson's r correlation coefficient values for correlations among the time series and mass spectra of the PMF factors. Here, 1 = MO-OOA1, 2 = LO-OOA1, 3 = LO-OOA2, 4 = MO-OOA2, 5 = SFOA, 6 = HOA, 7 = COA; **(e)** box and whiskers plot showing the distributions of scaled residuals for each *m/z*; **(f)** time series of the measured mass and the reconstructed mass from the sum of the 6 factors; **(g)** time series of the variations in the residual (= measured – reconstructed) of the fit; **(h)** the Q/Q_{exp} for each point in time; **(i)** the Q/Q_{exp} values for each fragment ion.

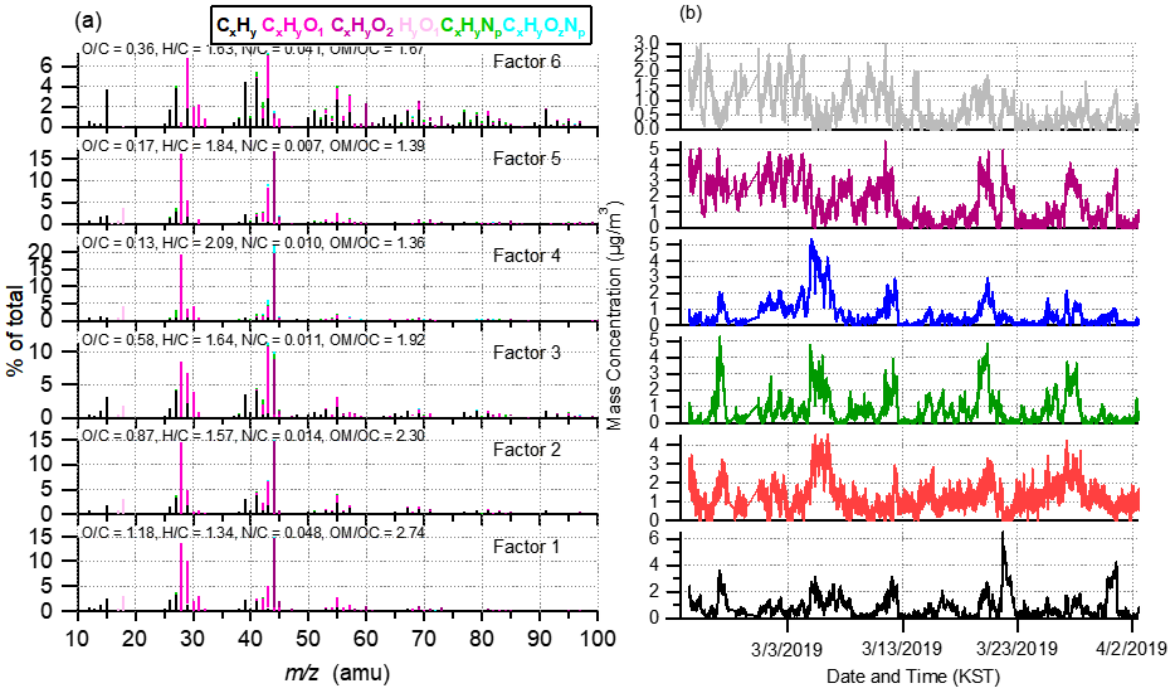

240

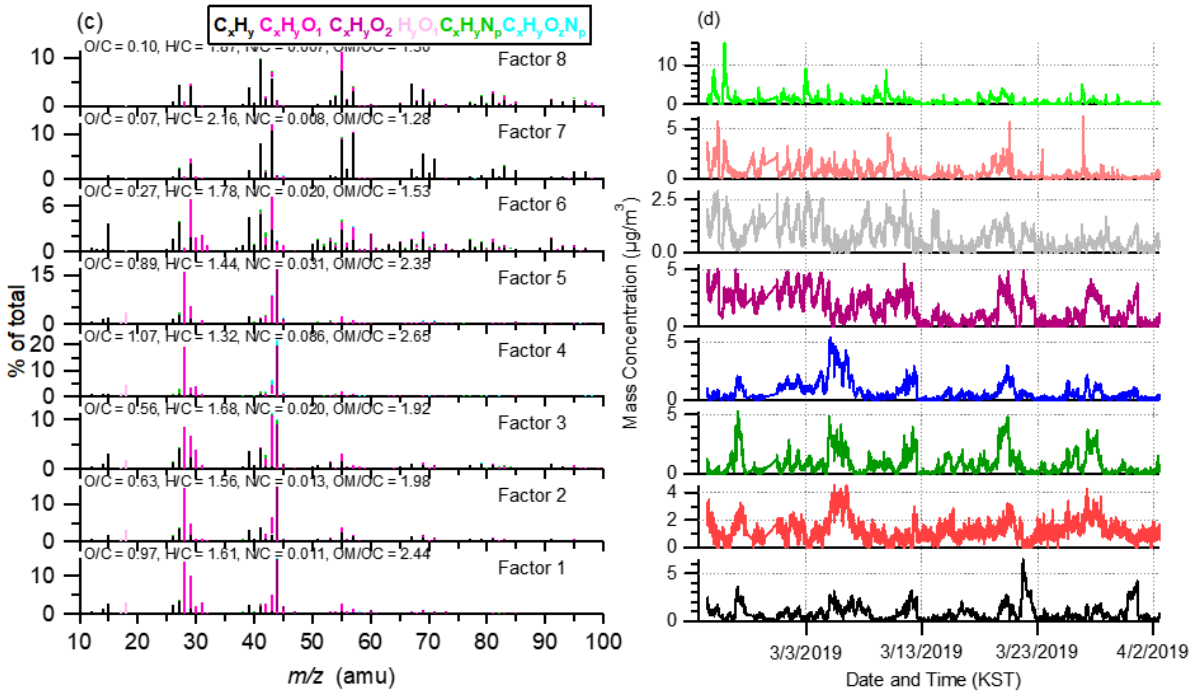

241

242

243

Figure S7. Overview of two other solution (6 factor and 8 factor solution) sets from PMF analysis: **(a)(b)** High resolution mass spectra and time series of the different OA factors from the 6-factor solution; **(c)(d)** High resolution mass spectra and time series of the different OA factors from the 8-factor solution

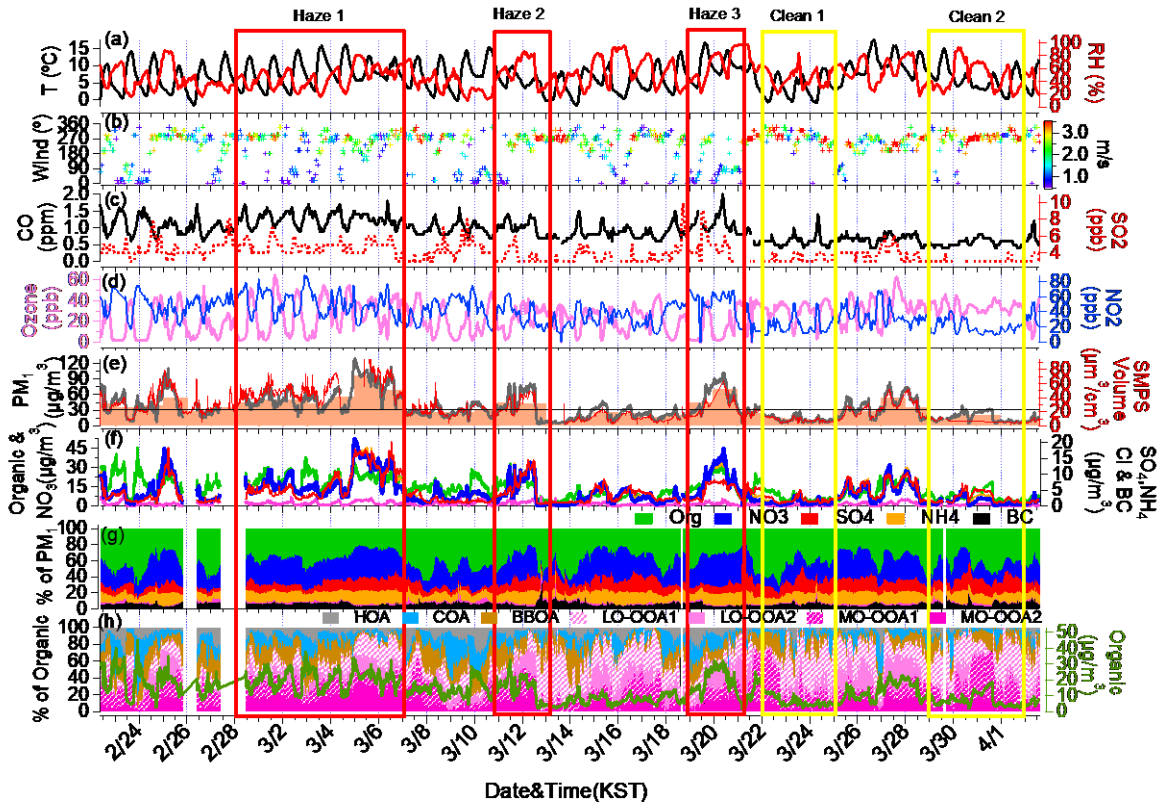

258

259

260 **Figure S8.** Overview of the temporal variations of submicron aerosols at the Korea Institute of
261 Science and Technology (KIST) in SMA from Feb. 22 to April 2 including three haze(red box)
262 and two clean (yellow box) period: **(a)** Time series of ambient air temperature (T) and relative
263 humidity (RH); **(b)** Time series of wind direction (WD), with colors showing different wind
264 speeds (WS); **(c)** Time series of CO and SO_2; **(d)** Time series of O_3, and NO_2; **(e)** Time series of
265 total particulate matter (PM_1), scanning mobility particle sizer (SMPS) volume concentrations
266 and also shown are the 24 h averaged PM_1+BC with bars. **(f)** Time series of the organic (Org.),
267 nitrate (NO_3^-), sulfate (SO_4^{2-}) , ammonium (NH_4^+) and BC aerosols; **(g)** Time series of the mass
268 fractional contribution of organic aerosols (Org.), nitrate (NO_3^-), sulfate (SO_4^{2-}), ammonium
269 (NH_4^+), chloride (Cl^-), and BC to total PM_1 together with isoprene and toluene time series; **(h)**
270 Time series of each factor derived from the positive matrix factorization (PMF) analysis

271

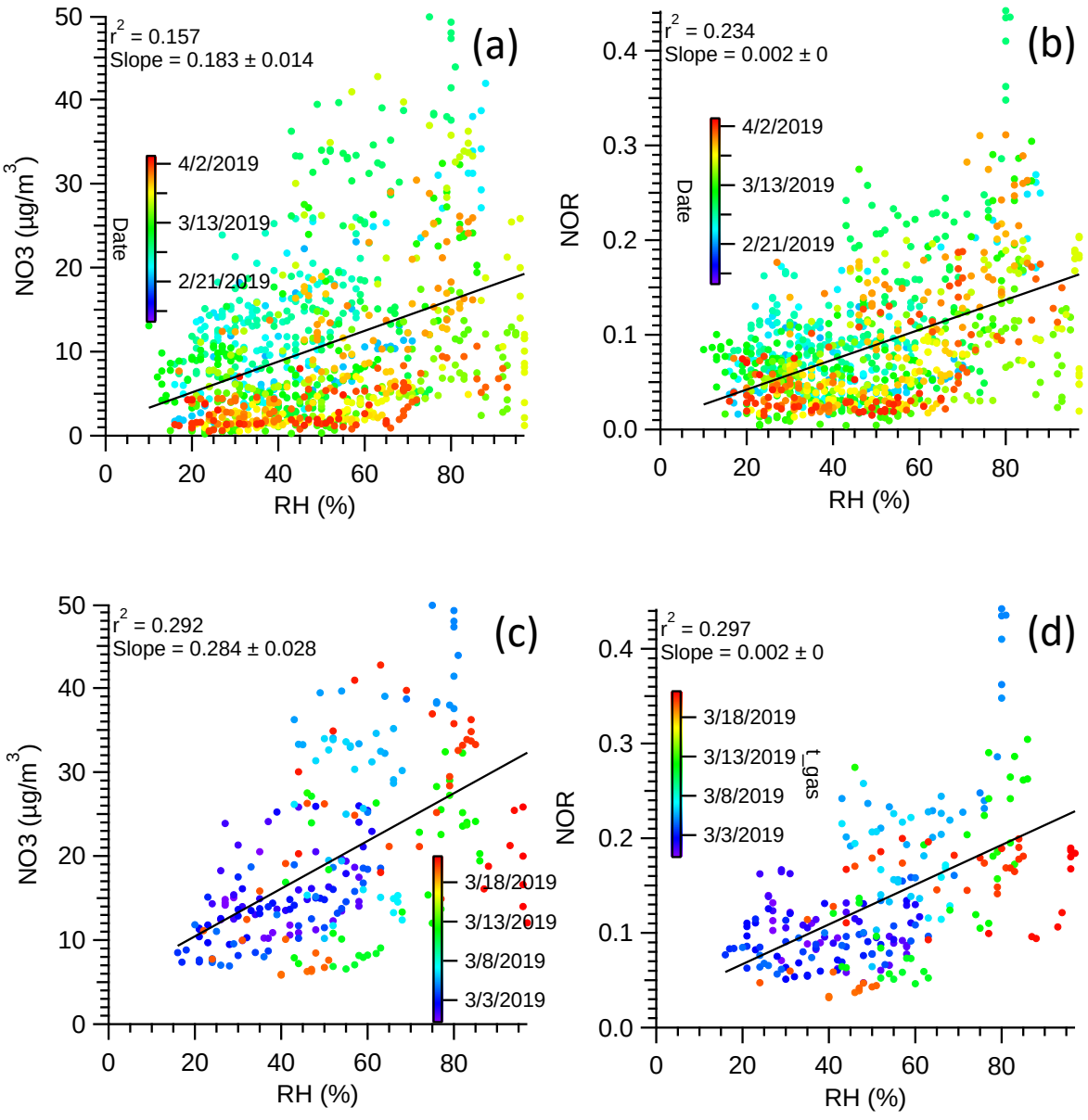

Figure S9. Scatterplot of the variations of nitrogen oxidation ratio (NOR) and NO3 as a function of RH **(a)(b)** during entire period; **(c) (d)** during haze period.

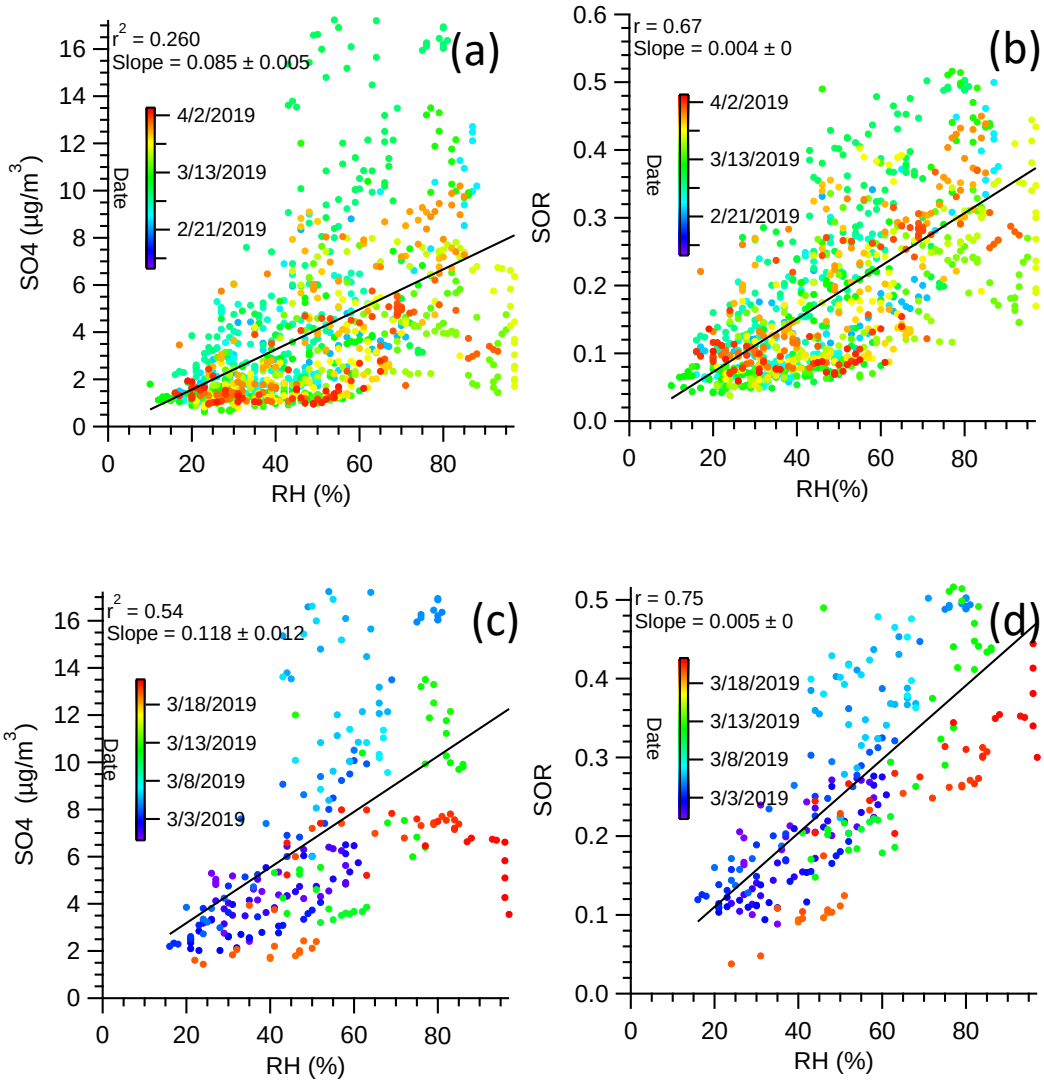

Figure S10. Scatterplot of the variations of sulfur oxidation ratio (SOR) and SO4 as a function of RH **(a)(b)** during entire period; **(c) (d)** during haze period.

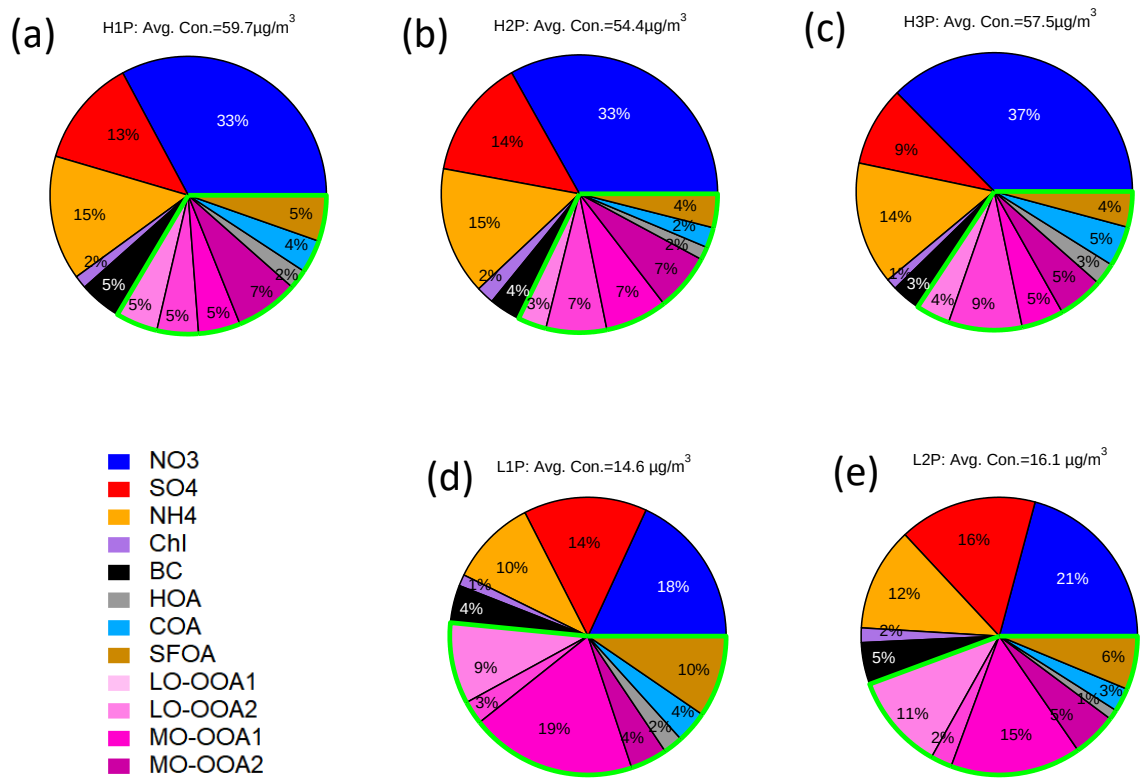

Figure S11. Averaged compositional pie chart of PM_1 species (non-refractory-PM_1 plus black carbon (BC)) in **(a-c)** three haze episodes and **(d, e)** two clean periods.

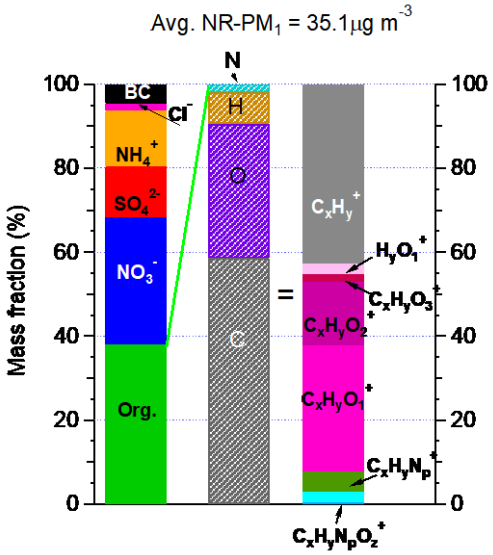

Figure S12. Overview of the OA compositions in SMA during entire study (early spring of 2019)

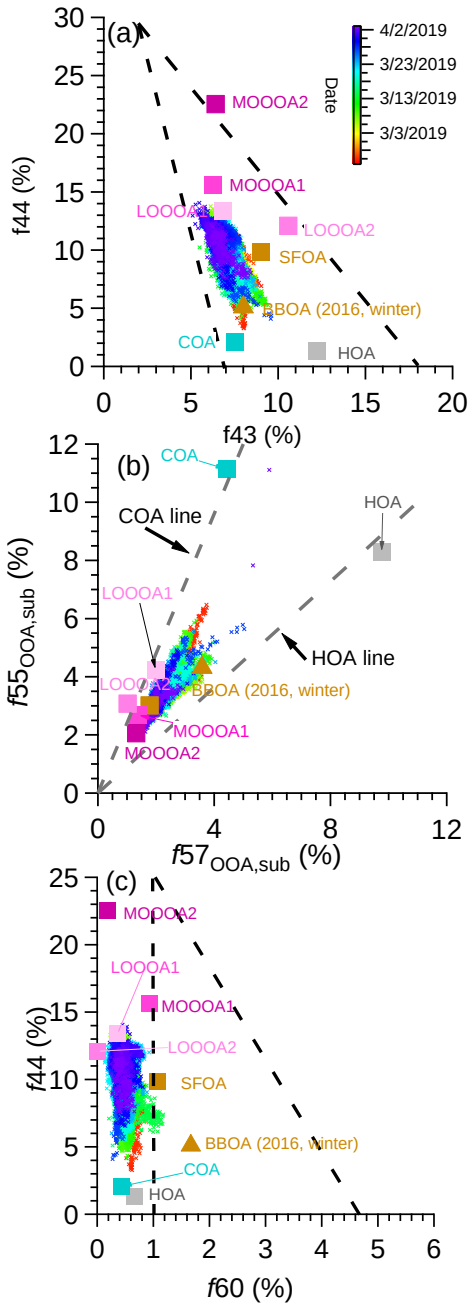

Figure S13. Triangular plots of **(a)** f_{44} versus f_{43} **(b)** $f_{55,\mathrm{OOA\ sub}}$ versus $f_{57,\mathrm{OOA\ sub}}$ and **(c)** f_{44} versus f_{60} for the seven OA factors and all of the measured OA data (dots), colored by date. f_{43}, f_{44}, and f_{60} are the ratios of the organic signal at *m/z* = 43, 44, and 60 to the total organic signal in the component mass spectrum, respectively. $f_{55,\mathrm{OOA\ sub}}$ and $f_{55,\mathrm{OOA\ sub}}$ are the ratios of the organic signal at m/z 55, 57 after subtracting the contributions from LO-OOA1, LO-OOA2, MO-OOA1

and MO-OOA2(e.g., $f_{55,\text{OOA sub}}$ = *m/z* 55 - *m/z55*$_{LO\text{-}OOA1}$ - *m/z55*$_{LO\text{-}OOA2}$ - *m/z55*$_{MO\text{-}OOA\ 1}$- *m/z55*$_{MO\text{-}OOA2}$; $f_{57,\text{OOA sub}}$ = *m/z* 57- *m/z57*$_{LO\text{-}OOA1}$- *m/z57*$_{LO\text{-}OOA2}$ - *m/z57*$_{MO\text{-}OOA1}$ - *m/z57*$_{MO\text{-}OOA2}$). 2016 winter BBOA is also shown with triangle for comparison (Kim et al., 2017)

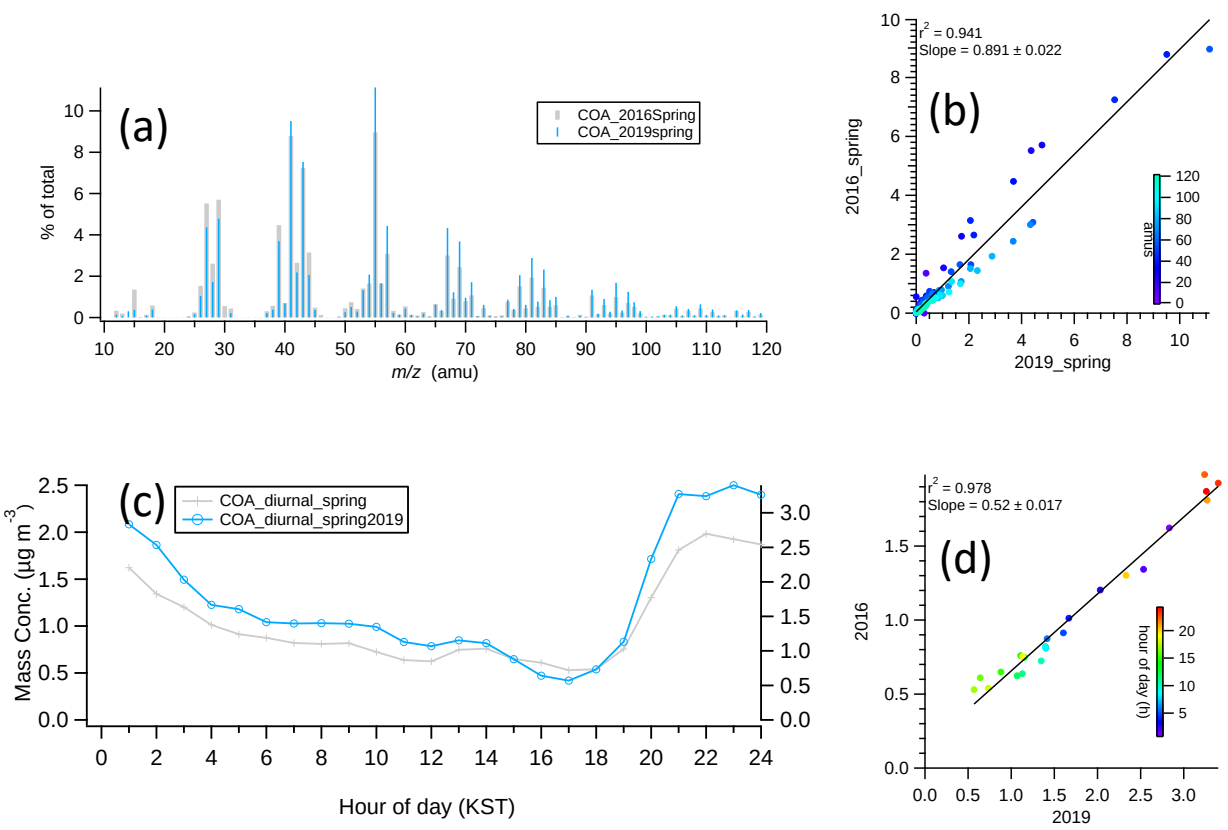

Figure S14. (a) mass spectra of the COAs from this study (spring) and the one from KORUS-AQ (Kim et al., 2018); **(b)** scatter plots of both COA mass spectra; **(c)** diurnal profile of the COAs from this study (spring) and the one from KORUS-AQ (Kim et al., 2018);and **(d)** scatter plots of both COA diurnal profile.

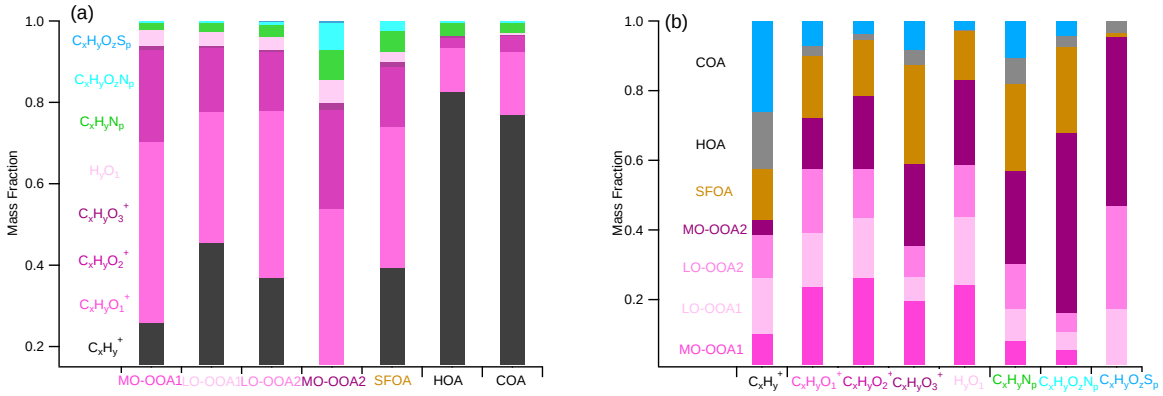

Figure S15. (a) Average mass fractional contributions of seven ion families to each of the OA factors and; **(b)** Average mass fractional contributions of seven OA factors to each ion family

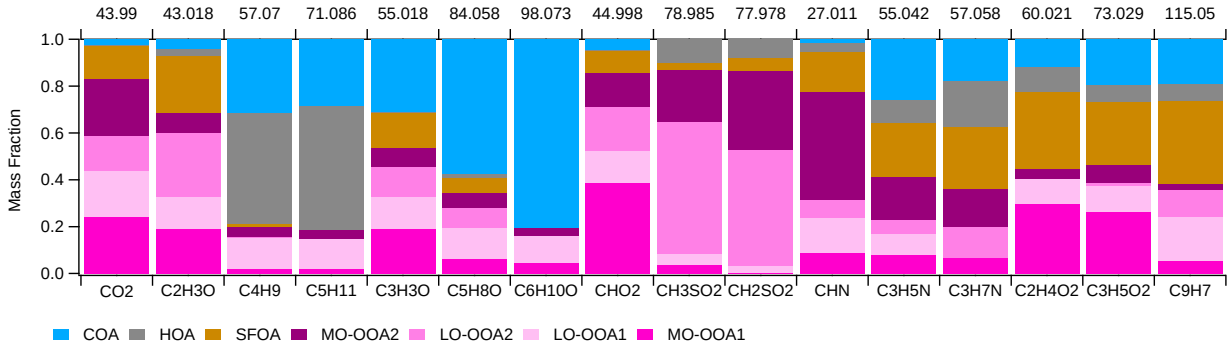

Figure S16. Mass fractional contribution of the seven factors from PMF analysis to various ions that are relevant to each significant tracer.

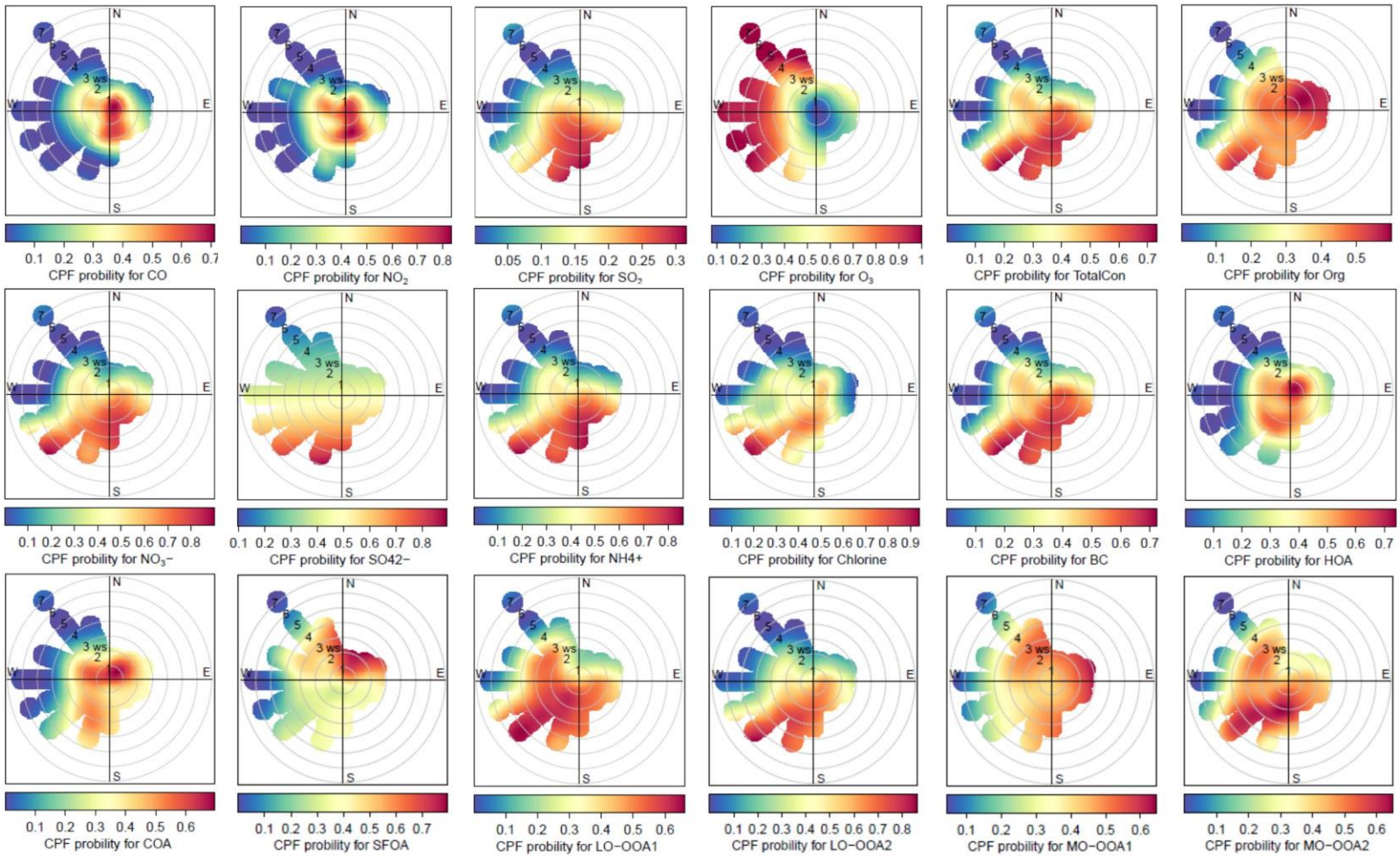

Figure S17. Conditional probability function (CPF) of hourly averaged total PM_1 +BC, BC and mixing ratios various gas phase species concentrations (top row), hourly averaged total PM_1 species (middle row), and mass concentrations of the seven OA factors identified from PMF analysis (bottom row) as a function of WS and direction. Color is defined as *my/ny*, where *my* is the number of samples in the wind sector y with mixing ratio greater than the 50 percentile concentration, and *ny* is the total number of samples in the same wind sector.

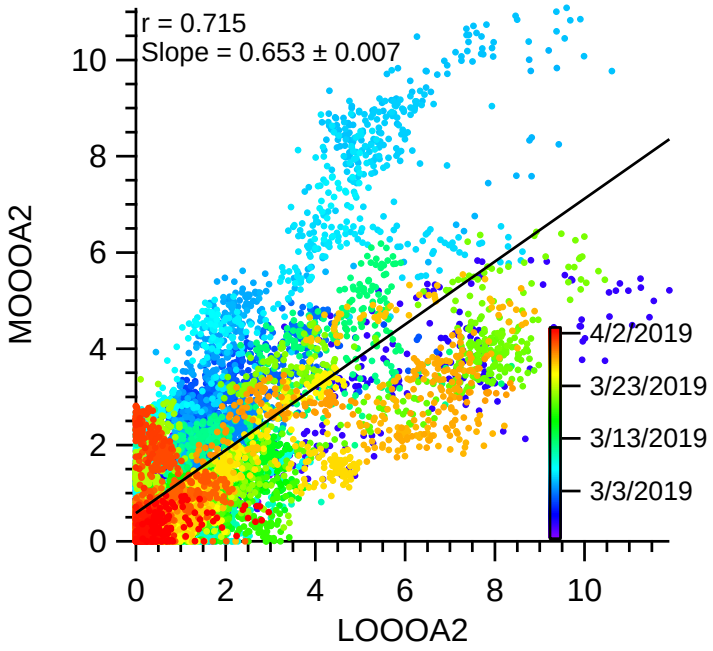

Figure S18. Correlations between MO-OOA2 and LO-OOA2 colored by date.

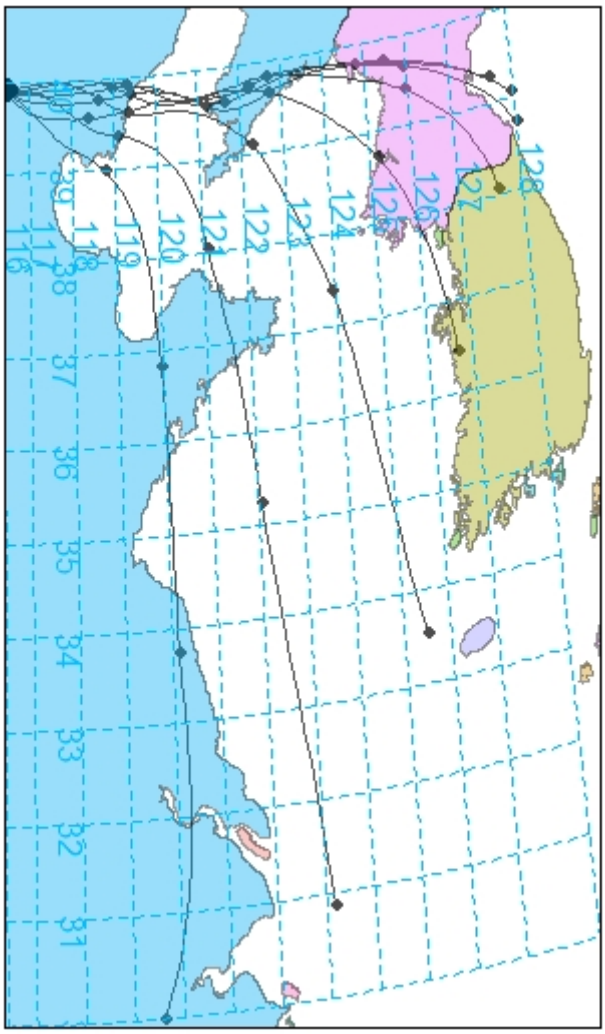

Figure S19. Forward trajectory from Beijing measurement site. Each vertical and horizontal blue dotted line indicate longitude and latitude, respectively. Each black point indicate the endpoint of air parcel movement during 12 h.

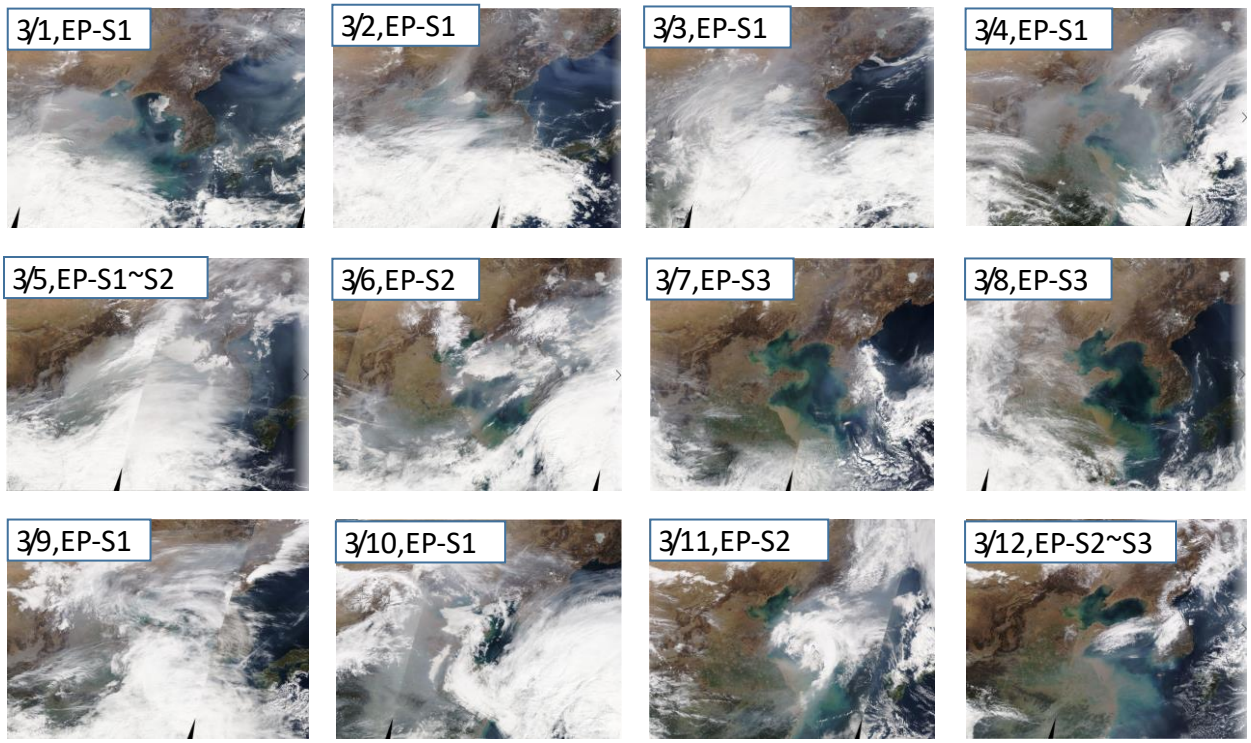

Figure S20. Long range transportation of plums from China to Korea during Haze period. Plots are from MODIS, terra. Corresponded haze episode and stages are labeled left top of the figure.

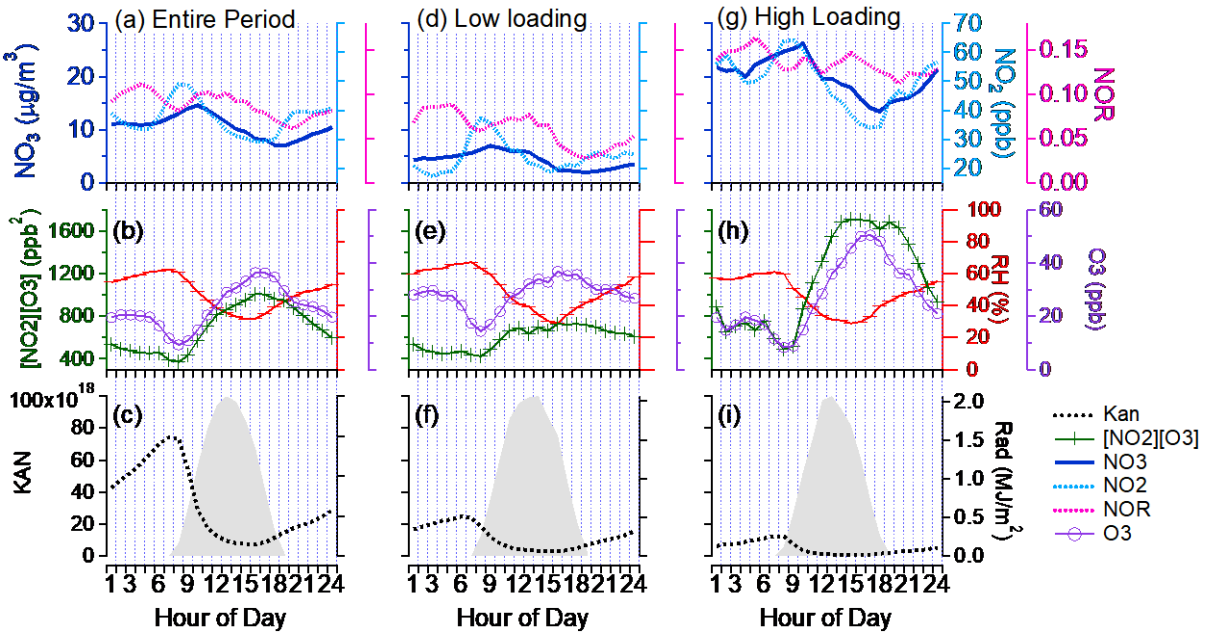

Figure S21. One-hour averaged diurnal profiles for nitrate and various parameters and proxies for formation pathways in (a-c) entire period (d-f) low loading period and (g-i) high loading period during 2019 spring. One-hour averaged diurnal profiles of NO_2, NO_3, NOR (nitrate oxidation ratio) are shown in top row; $[NO_2][O_3]$ as a proxy for nighttime formation of HNO3, RH and one-hour averaged O_3 are shown in middle row; and KAN as the equilibrium constant for gas-to-particle partitioning for ammonium nitrate and solar radiation are shown at the bottom row.

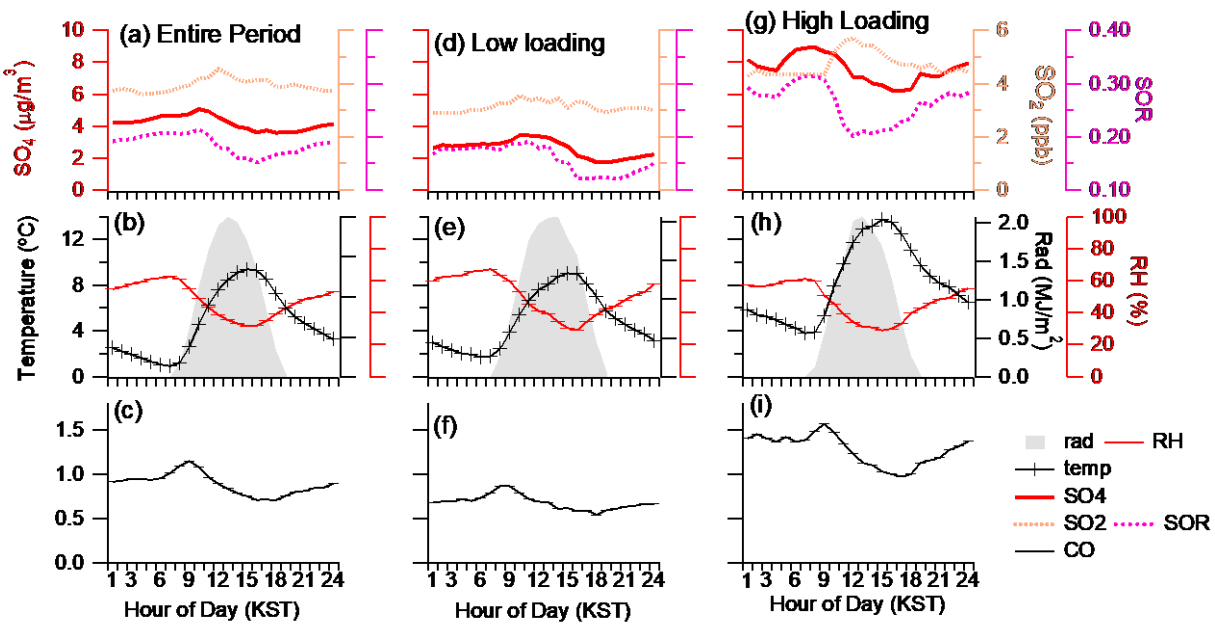

Figure S22. One-hour averaged diurnal profiles for sulfate and various parameters and proxies for formation pathways in entire, haze and clean period during 2019 spring; Temperature, relative humidity and solar radiation as a proxy for daytime H_2SO_4 formation in (a-c) entire period (d-f) low loading period and (g-i) high loading period.

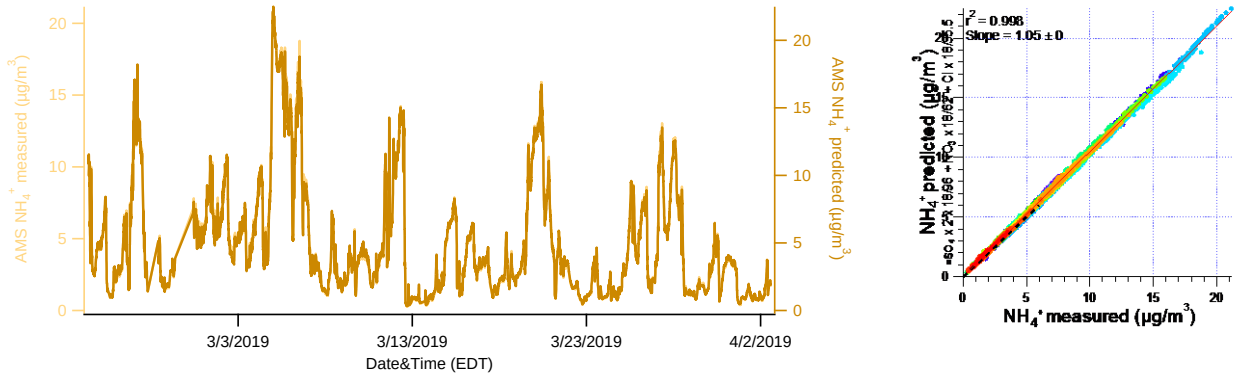

Figure S23. Time series (a) and Scatterplot (b) that compares predicted NH_4^+ versus measured NH_4^+ concentrations. The predicted values were calculated assuming full neutralization of the anions (e.g., sulfate, nitrate, and chloride). The data points are colored by date.

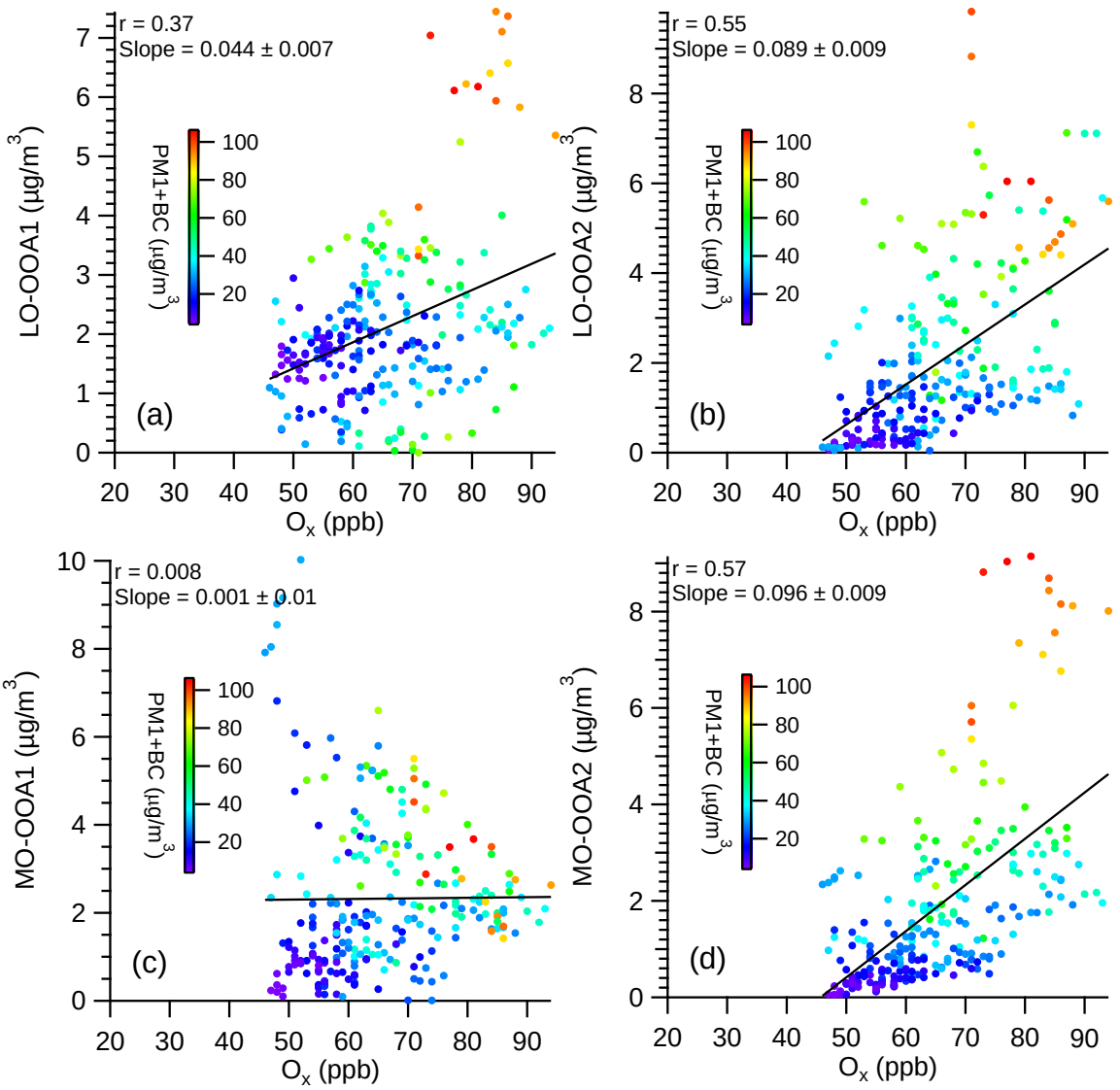

Figure S24. Time series (a) LO-OOA1; (b) LO-OOA2; (c) MO-OOA1; (d) MO-OOA2 vs O_x during the daytime (10:00 - 16:00) in the early spring of 2019.

References

Aiken, A. C., Decarlo, P. F., Kroll, J. H., Worsnop, D. R., Huffman, J. A., Docherty, K. S., Ulbrich, I. M., Mohr, C., Kimmel, J. R., Sueper, D., Sun, Y., Zhang, Q., Trimborn, A., Northway, M., Ziemann, P. J., Canagaratna, M. R., Onasch, T. B., Alfarra, M. R., Prevot, A. S. H., Dommen, J., Duplissy, J., Metzger, A., Baltensperger, U., and Jimenez, J. L.: O/C and OM/OC ratios of primary, secondary, and ambient organic aerosols with high-resolution time-of-flight aerosol mass spectrometry, Environmental Science & Technology, 42, 4478-4485, 10.1021/es703009q, 2008.

Canagaratna, M. R., Jimenez, J. L., Kroll, J. H., Chen, Q., Kessler, S. H., Massoli, P., Hildebrandt Ruiz, L., Fortner, E., Williams, L. R., Wilson, K. R., Surratt, J. D., Donahue, N. M., Jayne, J. T., and Worsnop, D. R.: Elemental ratio measurements of organic compounds using aerosol mass spectrometry: characterization, improved calibration, and implications, Atmospheric Chemistry and Physics, 15, 253-272, 10.5194/acp-15-253-2015, 2015.

Kim, H., Zhang, Q., Bae, G. N., Kim, J. Y., and Lee, S. B.: Sources and atmospheric processing of winter aerosols in Seoul, Korea: insights from real-time measurements using a high-resolution aerosol mass spectrometer, Atmos. Chem. Phys., 17, 2009-2033, 10.5194/acp-17-2009-2017, 2017.

Kim, H., Zhang, Q., and Heo, J.: Influence of intense secondary aerosol formation and long-range transport on aerosol chemistry and properties in the Seoul Metropolitan Area during spring time: results from KORUS-AQ, Atmos. Chem. Phys., 18, 7149–7168, https://doi.org/10.5194/acp-18-7149-2018, 2018.

Kuwata, M., Zorn, S. R., and Martin, S. T.: Using Elemental Ratios to Predict the Density of Organic Material Composed of Carbon, Hydrogen, and Oxygen, Environmental Science & Technology, 46, 787-794, 10.1021/es202525q, 2012.

Middlebrook, A. M., Bahreini, R., Jimenez, J. L., and Canagaratna, M. R.: Evaluation of Composition-Dependent Collection Efficiencies for the Aerodyne Aerosol Mass Spectrometer using Field Data, Aerosol Science and Technology, 46, 258-271, 10.1080/02786826.2011.620041, 2012.

Zhang, Q., Canagaratna, M. R., Jayne, J. T., Worsnop, D. R., and Jimenez, J. L.: Time- and size-resolved chemical composition of submicron particles in Pittsburgh: Implications for aerosol sources and processes, Journal of Geophysical Research-Atmospheres, 110, 10.1029/2004jd004649, 2005.